Spin and energy relaxation in germanium studied by spin-polarized direct-gap photoluminescence

Fabio Pezzoli,[1,*] Lan Qing,[2,*] Anna Giorgioni,[1] Giovanni Isella,[3] Emanuele Grilli,[1] Mario Guzzi,[1] and Hanan Dery[2,4]

[1]*LNESS-Dipartimento di Scienza dei Materiali, Università degli Studi di Milano-Bicocca,*
via R. Cozzi 53, I-20125 Milano, Italy

[2]*Department of Physics and Astronomy, University of Rochester, Rochester, New York 14627, USA*

[3]*LNESS-Dipartimento di Fisica del Politecnico di Milano, Polo di Como, via Anzani 42, I-22100 Como, Italy*

[4]*Department of Electrical and Computer Engineering, University of Rochester,*
Rochester, New York 14627, USA

Spin orientation of photoexcited carriers and their energy relaxation are investigated in bulk Ge by studying spin-polarized recombination across the direct band gap. The control over parameters such as doping and lattice temperature is shown to yield a high polarization degree, namely larger than 40%, as well as a fine tuning of the angular momentum of the emitted light with a complete reversal between right- and left-handed circular polarization. By combining the measurement of the optical polarization state of band-edge luminescence and Monte Carlo simulations of carrier dynamics, we show that these very rich and complex phenomena are the result of the electron thermalization and cooling in the multivalley conduction band of Ge. The circular polarization of the direct-gap radiative recombination is indeed affected by energy relaxation of hot electrons via the X valleys and the Coulomb interaction with extrinsic carriers. Finally, thermal activation of unpolarized L valley electrons accounts for the luminescence depolarization in the high temperature regime.

PACS number(s): 78.55.Ap, 78.20.−e, 75.25.−j, 85.75.−d

I. INTRODUCTION

The coupling between the angular momentum of photons and the spin angular momentum of carriers, termed optical orientation,[1,2] has so far been recognized as one of the main challenges in group IV materials.[2–4] The poor absorption and emission efficiencies, associated with the weak electric-dipole transitions of the fundamental indirect gap of such semiconductors, jeopardized the optical exploitation of their rich spin physics. Indeed, silicon and germanium feature lattice inversion symmetry and predominant spinless isotopes,[2,5] yielding long spin coherence times.[5,6] This feature is crucial for the effective implementation of spintronic devices,[7] and quantum information processing.[2,5,8]

Only very recently, however, the quasidirect behavior of Ge has sparked interest in its photonic properties,[9,10] and stimulated the use of various optical schemes aiming at addressing its spin physics.[11–14] In Ge, the absolute minimum of the conduction band (CB) is at the L point of the Brillouin zone, but there exists a local minimum at the zone-center Γ. At low temperature the former leads to an indirect energy gap of 0.744 eV[15] and the latter to a direct gap of 0.898 eV.[15] Optical orientation via absorption of circularly polarized photons at the direct energy gap can then be exploited to readily investigate the spin properties of Ge.[16–19] Noticeably, spin-polarized electrons optically pumped in the Γ valley can conserve their spin during ultrafast scattering to the lower energy L valleys,[14] which are responsible for charge and spin transport. Such a mechanism, which is absent in the widely studied III-V semiconductors, makes Ge spin dynamics very rich. In addition, it provides a viable approach to inject spin-polarized carriers in Ge without relying on ferromagnetic gate stacks, which are prone to low efficiency and experimental artifacts due to defects and localized interfacial states.[20,21]

Optical orientation has indeed recently allowed progress in the investigation of spin dynamics of both electrons and holes in bulk Ge. Spin relaxation times of holes have been shown to be below 1 ps,[17] whereas electron spin relaxation times are in the nanosecond range below 200 K.[13,22,23] Yet very little is known about spin flip scattering by dopants and the role played by impurities in determining spin dynamics in different temperature regimes.[24,25]

Inspired by the quasi-direct-gap behavior of Ge and by the possibility to optically initialize spins, we report in this work a spin-polarized photoluminescence (PL) study focused on the recombination across the direct gap of bulk Ge over a wide doping and temperature range. We directly measured the polarization state of the direct-gap emission by means of Stokes analysis,[26] shedding light on the optical orientation process and on the interplay between energy and spin relaxation channels. The role of carrier thermalization and cooling in determining luminescence polarization in Ge are disclosed by Monte Carlo simulations, in which nonequilibrium kinetics of photoexcited electrons is used to extract the circular polarization degree of the emitted light under steady state conditions.

Our analysis shows that in Ge the state of light polarization of the direct-gap emission is governed by kinetics of spin-polarized electrons, highlighting the role of energy relaxation of hot electrons within the X valleys. The direct comparison between theory and experiments points out that above 170 K backscattering of unpolarized electrons from L to Γ valley leads to a decay of the circular polarization degree of direct-gap emission, no matter the doping of the bulk samples. Remarkably, at temperatures below 170 K a complete reversal of the helicity of light polarization can be obtained either by changing the doping level or the lattice temperature. In addition, a maximum in the polarization degree of the emitted light is obtained around 100–150 K, reaching in intrinsic Ge samples surprisingly high values, i.e., larger than 40%.

Such puzzling behavior stems for the complex carrier dynamics taking place in the multivalley band structure of Ge, where the electron spin (and ensuing direct-gap luminescence polarization) is dictated by cooling of hot electrons via Coulomb collisions and intervalley scattering between Γ, X, and L valleys.

The paper is organized as follows. In Sec. II we discuss the samples and their optical properties, extending the results to the polarimetric analysis of the PL. In Sec. III we describe in detail the Monte Carlo simulations. These calculations unravels energy and spin relaxation channels, finally disclosing their relative contribution in determining the experimental findings. After having discussed in Sec. IV the physics underlying the observed phenomena, we then in Sec. V summarize the results and provide the future perspectives of this work.

II. EXPERIMENTS

A. Experimental details

We studied a set of bulk Ge(001) samples having a different type and level of doping: (i) a p-type Ge:Ga wafer, with an acceptor concentration of 3.6×10^{18} cm^{-3}, named p^+-Ge, (ii) a n-type Ge:As, $6°$ miscut, with a donor concentration of 8.3×10^{16} cm^{-3}, named n-Ge, (iii) a p-type wafer with a doping concentration of 1.4×10^{15} cm^{-3}, named p^--Ge, and (iv) an intrinsic Ge sample, with a resistivity of 47 Ω cm, named i-Ge. The doping levels have been obtained by means of room temperature resistivity measurements. Sample characteristics are summarized in Table I.

PL measurements were carried out in backscattering geometry in the temperature range between 4 and 300 K. The samples were excited by a Nd : YVO$_4$ laser. The excitation energy was 1.165 eV and the light was left-handed circularly polarized (σ^-). The laser spot size on the sample surface was about 100 μm, resulting in a power density of $\sim$1 kW/cm^2. The polarization state of the luminescence was probed by a Stoke analyzer, i.e., an optical retarder followed by a linear polarizer. Hereafter we define the analyzer angle as the angle determined by the optical axis of the polarizer and that of the retarder. In the experiments the analyzer angle spans $360°$ with a resolution of $1°$. PL was dispersed by a spectrometer equipped with a thermoelectrically cooled InGaAs array detector, with a cutoff starting at about 0.755 eV. The energy accuracy was $\sim$4 meV. The multiple-channel detector measured the amplitude of the PL spectra as a function of the analyzer angle. The analysis of the peak amplitude modulation provided the Stokes parameters S_i with $i = 0$–3, which permit the full characterization of the polarization state of light.[14,26,27] Since partially polarized light can be considered as a superposition of unpolarized and completely polarized

light, we can define the degree of polarization ρ as[26,27]

$$\rho = \pm \frac{\sqrt{S_1^2 + S_2^2 + S_3^2}}{S_0}. \tag{1}$$

For circularly polarized light, the sign of the polarization degree has been chosen to be consistent with the sign of the Stokes parameter S_3, which defines whether the light is left handed (σ^-): $-1 \leqslant S_3 < 0$, or right handed (σ^+): $0 < S_3 \leqslant 1$.

B. Photoluminescence

The PL spectra of bulk, undoped Ge(001) are outlined in Fig. 1(a). At 4 K, the spectral feature observed at 0.885 eV is the direct band gap emission, which is due to the recombination of holes with electrons, directly photogenerated within the Γ valley by the laser excitation at 1.165 eV. The lifetime of Γ electrons is dominated by their fast scattering out of the optically coupled region towards the side X and L valleys and limited to a few hundred femtoseconds.[30–33] The relaxation processes towards the bottom of the Γ valley are significantly slower than in typical III-V materials, where phonon scattering is driven by the efficient Fröhlich interaction, which is absent in Ge since the crystal bonds are purely covalent. In addition, the deformation potential interaction between long-wavelength optical phonons and CB electrons is weak in Ge due to the space inversion symmetry.[34] As a result, scattering to the side valleys is more efficient than the intravalley cooling at Γ.

The majority of electrons excited in the Γ valley will thus reach and dwell in the L valley, experiencing a relatively long lifetime τ_L between tens and hundreds of microseconds at room temperature.[35] The two main features shown in the lower panel of Fig. 1(a) at 0.737 and 0.715 eV can thus be ascribed to recombination between holes at Γ and L electrons mediated by transverse (TA) and longitudinal (LA) acoustic phonons, respectively.[36] By increasing the temperature these two PL bands redshift, leaking out of the spectral response range of the detector except for their high energy tail [see upper panel of Fig. 1(a)]. The indirect-gap emission will not be discussed further, since in this work we focus on the spin and energy relaxation of electrons directly photoexcited in the Γ valley. Finally, we point out that the weak feature observed in Fig. 1(a) at about 1.056 eV is almost temperature independent and can be ascribed to resonant intervalence-band Raman scattering.[37,38]

As shown in Fig. 1(a) by the color-coded map of the PL intensity, the direct-gap emission redshifts with increasing the lattice temperature, as a result of the band gap shrinkage. Above 125 K it is superimposed to the high energy tail of the indirect-gap PL. The observed peak position of the direct band gap emission is in good agreement with the temperature dependence of the gap as described by Varshni's law,[28] reported as a solid line in Fig. 1(b).

By sweeping the sample temperature, while keeping fixed the excitation energy E_{exc}, we gather spectroscopic access to high energy states within the bands. Holes (electrons) are excited in the VB (CB) with a total excess energy $\Delta E = E_{exc} - E_0$, which increases with the temperature [see Fig. 1(c)]. E_0 is the energy of the direct gap. It is worth noticing that already in the low temperature range, the excess energy

TABLE I. Ge bulk samples investigated in this work.

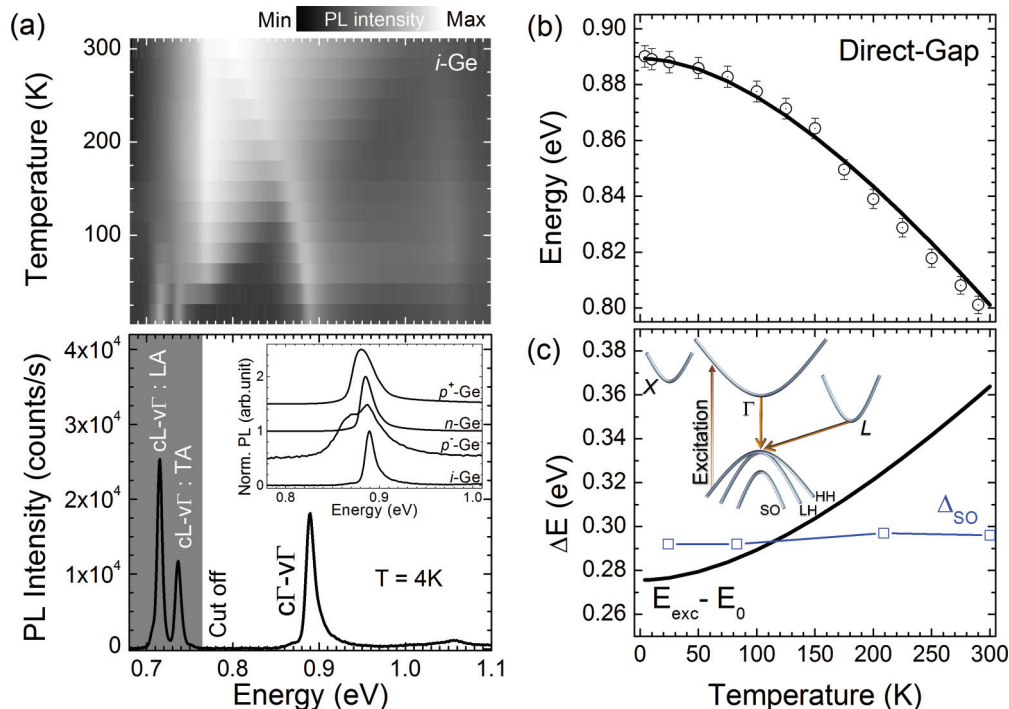| Sample	Resistivity (Ω cm)	Doping (cm^{-3})
p^+	0.0046	3.6×10^{18}
n	0.358	8.3×10^{16}
p^-	2.39	1.4×10^{15}
i	47	$\approx 10^{13}$

FIG. 1. (Color online) (a) Upper panel: Color-coded map of the PL intensity describing the temperature dependence of the photoluminescence (PL) spectra of i-Ge. Lower panel: 4 K PL data. Direct-gap, $c\Gamma - v\Gamma$, and indirect-gap transitions, $cL - v\Gamma$, mediated by longitudinal (LA) and transverse (TA) acoustic phonons are indicated along with the detector cutoff. The 4K PL spectra from all the studied samples are reported in the inset. (b) Energy variation of the direct gap with the temperature. Open dots are the PL peak positions measured in i-Ge, whereas the solid line represents Varshni's law according to the parameters of Ref. 28. (c) Temperature dependence of the total excess energy ΔE for carriers photoexcited in Ge by a laser energy at 1.165 eV (solid black line). The blue squares show the variation of the energy of the split-off band Δ_{SO} with temperature according to Ref. 29. The inset shows the physical processes underlying the luminescence mechanisms.

for CB electrons is comparable to the energy difference of the Γ and X valley bottoms, $\delta\epsilon_{x,\Gamma} \approx 0.04$ eV, thus activating scattering to the side X valleys as an energy relaxation channel. Moreover, the threshold for optical transitions involving the split-off band (SO), lying at $\Delta_{SO} \sim 0.29$ eV below the VB edge,[29] is approached at about 125 K. At low temperatures electrons can indeed be photogenerated from the SO band directly at the bottom of the CB, whereas the vast majority of high energy electrons, promoted far above the CB edge, result from optical transitions from heavy hole (HH) states at the top of the VB. The oscillator strength for transitions at $k = 0$ involving HH states is three times the one involving light hole (LH) states.

The 4 K spectra of the doped samples [see inset of Fig. 1(a)] show that at a fixed temperature and as impurities are introduced in the Ge host crystal, the direct gap shifts to lower energies, the shift being larger for samples with a larger doping level.[37,39] We point out that the low energy feature observed at about 0.87 eV in p^--Ge quenches with the temperature and it can be tentatively attributed to recombination of carriers bound to shallow states. Hereafter, we focus on the samples with the lowest and the highest doping level: i-Ge and p^+-Ge, respectively, to pin down the impact of doping on the PL spectra.

The PL analysis can reveal important features related to the different phenomena taking place on the photoexcited carriers in doped samples. Indeed the spectral dependence

of the direct-gap PL is the result of the joint density of states weighted by the distribution function of carriers, finally leading to a skewed line shape. We thus modeled the line shape of the PL spectra by using the following exponentially modified Gaussian distribution, i.e., the convolution of an exponentially decaying function and a normal distribution[40]:

$$\Phi(E) = \frac{A}{\lambda} \exp\left[\frac{1}{2}\left(\frac{w}{\lambda}\right)^2 - \frac{E - E_{\max}}{\lambda}\right]$$
$$\times \int_{-\infty}^{z} \frac{1}{\sqrt{2\pi}} \exp\left(-\frac{x^2}{2}\right) dx, \qquad (2)$$

where

$$z = \frac{E - E_{\max}}{w} - \frac{w}{\lambda}, \qquad (3)$$

E is the photon energy, $E_{\max}$ is the PL peak position, and A is the amplitude of the PL band. w is the width of the Gaussian component, which allows us to estimate inhomogeneous broadening effects, while λ is the modification or skewness factor, which quantifies the asymmetry in the line shape due to the thermal distribution of carriers in the band. The latter two parameters thus provide valuable information about the population of the carriers which experience radiative recombination from the Γ valley.

The results of the modeling of the experimental data according to Eq. (2) are summarized in Fig. 2 highlighting λ and w in the low temperature range, i.e., where the line shape
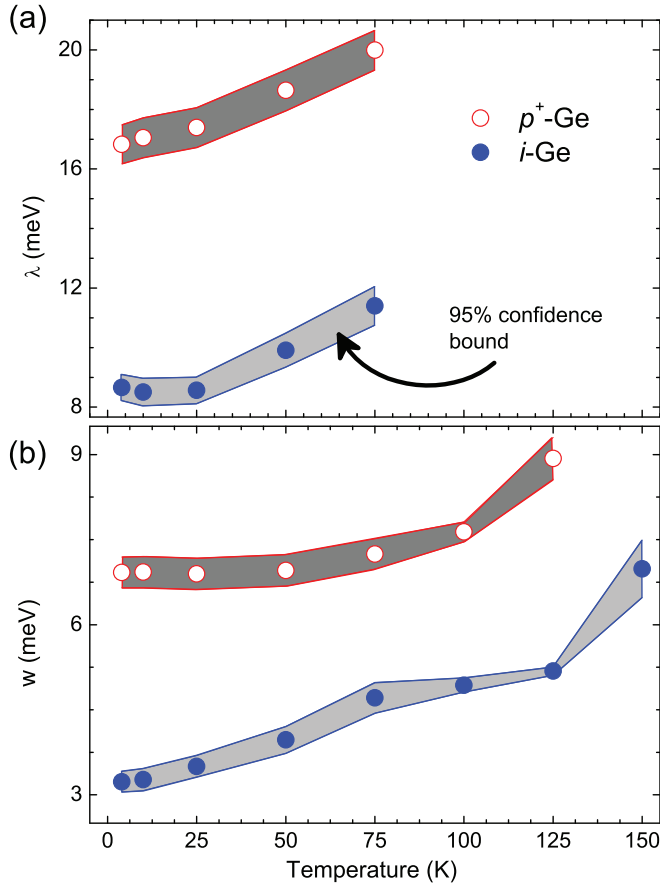
FIG. 2. (Color online) Temperature dependence of the modification factor λ and linewidth w of the direct-gap PL of p^+-Ge (open dots) and i-Ge (full dots) samples. The shadowed gray area defines the 95% confidence bound region as obtained from the fitting of the spectra with the exponentially modified Gaussian function reported in Eq. (2).

analysis is less affected by the tail of the indirect-gap emission. Noticeably, the average carrier temperature, elucidated by the skewness factor shown in Fig. 2(a), increases sharply above ≈ 50 K in the investigated samples. We therefore expect hot carrier phenomena and carrier-carrier interactions to play a major role in determining spin relaxation for temperatures above ≈ 50 K. Finally, as expected from band filling effects, Fig. 2(b) demonstrate that the PL linewidth increases with the concentration of extrinsic carriers.

C. Polarization-resolved photoluminescence

To address optical orientation of spins and their depolarization channels in Ge, we measured the polarization state of the direct-gap emission by means of the Stokes analysis.[14,26,27]

Zone-center valence band (VB) states transform with the same symmetry operations of atomic p orbitals and are characterized by a total angular momentum quantum number $J = 3/2$ (for HH and LH) and $J = 1/2$ (for SO states). The projection of the total angular momentum along the quantization axis, conveniently chosen to be parallel to the angular momentum of the exciting light beam, is $J_z = \pm 3/2$ for HH and $J_z = \pm 1/2$ for LH and the SO band. CB states at Γ are s-like and their total angular momentum coincide with

their spin and are labeled by $J = 1/2$ and $J_z = \pm 1/2$, i.e., $|J, J_z\rangle = |1/2, \pm 1/2\rangle$.

In a bulk material under external illumination with left-handed (σ^-) circularly polarized light, both final CB states $J_z = +1/2$ and $J_z = -1/2$ are populated, with a relative weight which depends upon the excitation energy,[16] and the strength of the dipole allowed transitions involved in the absorption process. The photogenerated spin-polarized carriers will then diffuse within the sample, possibly experiencing spin relaxation prior to radiative recombination. Spin relaxation mechanisms tend to equalize spin-up and spin-down populations. In bulk material, spin relaxation for holes is faster than for electrons because of the strong mixing of the HH and LH states.[2,41] As a result, under steady state conditions, the nonequilibrium electron spin population will govern the helicity and polarization degree of the direct-gap emission. Studies of the circular polarization of luminescence have allowed the investigation of spin physics of nonequilibrium carriers in direct-gap semiconductors such as GaAs, whereas no detailed studies have been reported so far for bulk Ge.[2] The similarity between the band structure of Ge and of III-V compounds near the center of the Brillouin zone lead to analogous optical orientation during the absorption process.[16] On the other hand, the ultrafast lifetime of Γ valley electrons in Ge, and the role played by scattering to the side valleys, can possibly lead to crucial differences in the spin relaxation channels and eventually in the luminescence polarization of direct-gap radiative recombination.

Figure 3(a) shows the contour plot of the direct-gap PL intensity as a function of the angle of the polarization analyzer at temperatures ranging from 4 K to room temperature. We can identify three regimes.

In the low temperature range, i.e., below ~ 90 K, for all the samples the amplitude modulation of the PL peaks reveals a sinusoidal behavior. According to Stokes analysis, this is the fingerprint of circularly polarized light and thus of optically oriented electron spins. Indeed the lifetime τ for electrons lying in the Γ valley of Ge is limited by the ultrafast scattering to the side valleys being hundreds of femtoseconds.[30,31] This process is much shorter than the spin relaxation time of CB electrons, $\tau_{es} \sim$ ns,[13,14,22,23] finally yielding circularly polarized luminescence. We recall that the observed luminescence polarization degree is $\rho \propto (1 + \tau/\tau_{es})^{-1}$.[42]

Remarkably, in both p^+-Ge and n-Ge the direct-gap PL is co-circular with respect to the excitation, having, under the experimental conditions, maxima (white areas) at $\pi/4 + n\pi$ and minima (black areas) at $3/4\pi + n\pi$.[43] Here $n = 0, 1$. The opposite holds for i-Ge and p^--Ge.

For $90 \leqslant T \leqslant 170$ K, the direct-gap PL is still circularly polarized. The helicity of photons emitted at the direct gap transition in p^+-Ge and n-Ge, i.e., samples with doping larger than 10^{16} cm^{-3}, turns out to be out of phase with respect to the one reported in the low temperature regime for the same samples. On the other hand, the helicity of the direct-gap emission in i-Ge and p^--Ge is not affected by the temperature variation, and it is co-circular with the one of the doped samples. In this temperature regime, the angular momentum of the direct-gap luminescence has the opposite direction as the one of the absorbed photons at the excitation energy. In addition, the amplitude of the peak modulation, and indeed
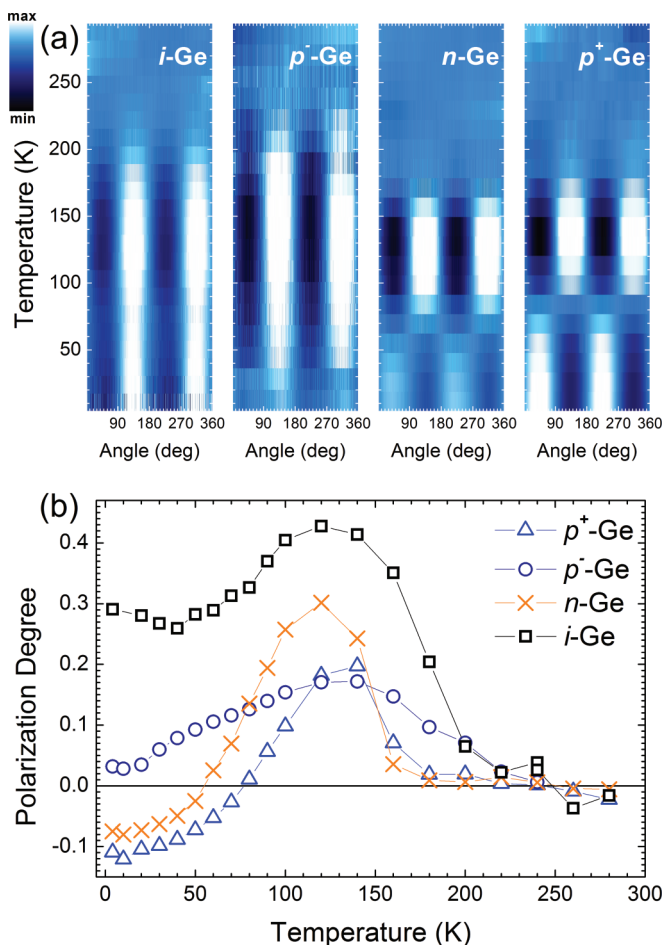
FIG. 3. (Color online) (a) Modulation of the peak intensity with the analyzer angle measured in i-Ge, p^--Ge, n-Ge, and p^+-Ge as a function of temperature. The minima (dark) and maxima (bright) are visible from the color-coded scale. (b) Experimental data for the polarization degree of the studied samples as a function of doping and temperature.

the polarization degree, is the largest for all the investigated samples.

Finally, in the high temperature range of Fig. 3(a), i.e., above ∼170 K, the aforementioned sinusoidal pattern is completely absent no matter the impurity content of the sample. This result demonstrates that the emitted light is not circularly polarized and that electron spins are no longer oriented prior to recombination. We can therefore conclude that above 170 K there exists a thermal activation of spin relaxation mechanisms. Such a process pertains to the material itself and not to the actual type and level of doping.

The findings discussed above are further corroborated by the temperature dependence of the polarization degree ρ of the emitted light [see Fig. 3(b)]. For all the investigated samples, ρ has a bell-shaped structure and, in agreement with the discussion above, ρ approaches zero at high temperatures. It should be noted that under the experimental conditions and according to the definition given in Eq. (4), ρ is negative for PL being co-circular with the excitation.

The impact of doping on the polarization degree is elucidated in Fig. 3(b) by the low temperature tail of ρ. Indeed at

4 K, $\rho \sim -10\%$ for both n-Ge and p^+-Ge, but it becomes positive when the impurity content is decreased below 10^{15} cm^{-3}, being few percent for p^--Ge and reaching a maximum of $\sim +30\%$ in i-Ge. In p^+-Ge and n-Ge, ρ changes sign between 50 and 90 K. Whereas in this temperature range ρ is almost constant for i-Ge and it slowly increases in p^--Ge. Noteworthy, ρ reaches a positive maximum around 125 K for all the samples, being larger than 40% in i-Ge. This is by far larger than the theoretical maximum of 25% achievable in complete absence of spin relaxation mechanisms for band-edge emission in direct-gap bulk materials.[2] Remarkably, such straightforward result can be obtained in Ge, as opposed to III-V compounds, without applying external perturbations, e.g., mechanical stress to remove VB degeneracy.

The puzzling dependence of ρ upon temperature and doping, reported in Fig. 3(b) for bulk Ge, does not have any counterpart in the well-established literature dealing with direct-gap semiconductors. Indeed, our experimental findings point out that mechanisms related to subtleties of the Ge band structure might play an important role in determining optical orientation as well as the spin dynamics. To address this further, we introduce the following theoretical analysis.

III. THEORY

We use Monte Carlo simulations to interpret the direct-gap PL in bulk Ge and to provide a solid, theoretical framework for the experimental results in the previous section. As shown in Fig. 4, these simulations fully recover the trends of the experiments for intrinsic p-type and n-type cases (without the use of fitting parameters). Below we elaborate on implementation of the numerical procedure and the description of the spin dynamics leading to the polarization of the direct-gap PL.

To achieve an accurate average of the direct-gap circular polarization degree, we simulate 10^9 photoexcited electrons. Each simulation ends if the electron reaches the bottom of the L valley or if it experiences direct-gap radiative recombination while spending time at the bottom of the Γ valley. Since the
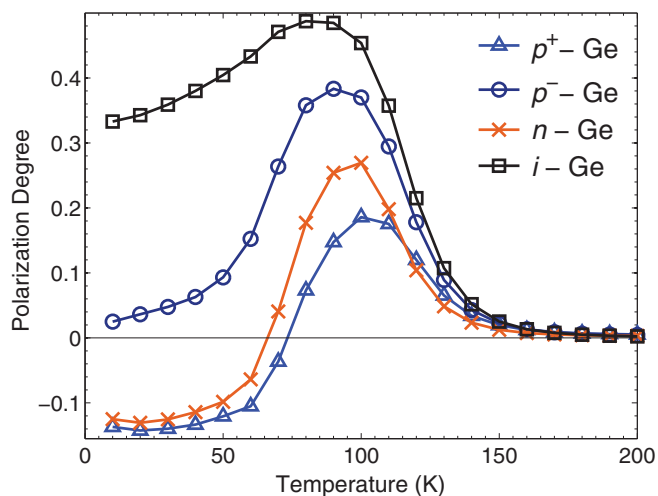

FIG. 4. (Color online) Calculated circular polarization degree of the recombination in the Γ valley of bulk Ge excited with σ^-.

vast majority of electrons relax to the bottom of the L valley, the use of 10^9 simulations guarantees accurate information on the small portion of electrons that experience direct-gap radiative recombination. The spin relaxation is not incorporated in these Monte Carlo simulations since the simulated dynamics mimics the evolution of the electrons within the first few picoseconds. However, due to the crosstalks between the populations of the different CB valleys, the high-temperature luminescence is governed by thermally activated electrons that reach to the Γ valley after spending a relatively long time in the L valleys (compared with the momentum, energy, and spin relaxation times).

To capture the radiative recombination from thermally activated and unpolarized electrons, the following considerations are taken. The probability of photoexcited electrons to reside in the L valley rather than to undergo luminescence in the Γ valley follows $\eta_1 \sim \tau_{r,\Gamma}/\tau_{\Gamma \to L}$, where $\tau_{r,\Gamma} \sim 0.1$ ns and $\tau_{\Gamma \to L} \sim 1$ ps are, respectively, the recombination time in the Γ valley and the scattering time from Γ to the L valley.[44] The photoexcited electrons with density N_e in steady state can also be calculated from the laser intensity and the absorption coefficient, which distribute mostly in the L valley bottom where doped electrons with density N_d may also exist. We denote their ratio as $\eta_2 \equiv N_d/N_e$. Most of these electrons eventually recombine with holes either in the L valley or in the Γ valley with thermal activation. The rates of the former and latter are, respectively, $\Gamma_a \sim \tau_{r,L}^{-1}$ and $\Gamma_b \sim \tau_{r,\Gamma}^{-1} \exp(-\Delta\epsilon_{\Gamma,L}/k_B T)$, where $\tau_{r,L} \sim 1$ μs is the recombination time in the L valley. Hence with the circular polarization degree of PL ρ_{MC} extracted from the Monte Carlo simulations within the time scale of momentum relaxation, we can derive the result with spin relaxation:

$$\rho \approx \frac{\rho_{MC}}{1 + \eta_1(1 + \eta_2)\dfrac{\Gamma_b}{\Gamma_a + \Gamma_b}}. \qquad (4)$$

The final results of Eq. (4) are depicted in Fig. 4. The dependence of the circular polarization degree on temperature and doping reconciles with the empirical results. It is mentioned that the thermal-activation process of unpolarized electrons form the L valley rather some unrealistic ultrafast spin relaxation in the Γ valley leads to the decay of the circular polarization degree at temperatures above 100 K for all the curves in Fig. 4. We now turn to the calculation procedure of the ultrafast electron evolution following photoexcitation from which we extract the value of ρ_{MC} in Eq. (4).

The photoexcitation is modeled by utilizing a pseudo-Voigt profile for the cw Nd:YVO$_4$ laser.[45] In addition, momentum alignment and spin-momentum correlation are found necessary to generate the electron distributions immediately after the photoexcitation.[46–48] The initial states of electrons are extracted from an eight-band Kane model.[49] For the momentum relaxation of photoexcited electrons, we incorporate all sorts of intervalley electron-phonon scattering between different L, X, or Γ valleys, and also intravalley scattering within each valley.[50,51] In addition, we consider the ionized impurity scattering, the carrier-carrier binary scattering, and the collective electron-plasmon scattering.[52] Below we elaborate on these details.

A. Photoluminescence in germanium

(a) *Band structure.* The CB of Ge includes four L valleys, one Γ valley, and six X valleys. In each valley we consider ellipsoidal constant energy surfaces as $\gamma(\mathbf{k}) = \epsilon(1 + \alpha\epsilon) = \hbar^2(k_l^2/m_l + k_t^2/m_t)/2$, where α is a nonparabolicity parameter,[53] and ϵ is the electron kinetic energy. l (t) denotes the longitudinal (transverse) components. We employ $m_l = 1.588m_0$, $m_t = 0.0815m_0$, $\alpha = 0.3$ eV^{-1} in the L valley, $m_l = 1.353m_0$, $m_t = 0.288m_0$, $\alpha = 0$ in the X valley, and $m_l = m_t = 0.037m_0$, $\alpha = 0$ in the Γ valley.[50] We introduce the Herring-Vogt transformation defined by $k_i^* = \mathcal{T}_{ij}^n k_i^n$.[54] In the frame of reference of the nth valley, centered at the bottom of the valley with the z axis along its symmetry axis, we take the transformation matrix $\mathcal{T}^n = \text{diag}(\sqrt{m_0/m_t}, \sqrt{m_0/m_t}, \sqrt{m_0/m_l})$ so that the ellipsoidal constant energy surfaces become spheres. To preserve vector equations, $\mathcal{T}^n$ is also applied to other vector quantities such as phonon wave vectors.

The band parameters of Ge vary slightly with temperature and doping. We adopt the dependence $E_{g,\Gamma}(T) = E_{g,\Gamma}(0) - \alpha_\Gamma T^2/(T + \beta_\Gamma)$ for the direct band gap,[28] where $E_{g,\Gamma}(0) = 0.887$ eV, $\alpha_\Gamma = 5.82 \times 10^{-4}$ eV/K, $\beta_\Gamma = 296$ K, and also $\Delta_{SO} = 0.287$ eV for the split-off energy. The band gap shrinkage takes 36, 9, and 1 meV for p-type 3.6×10^{18} cm^{-3} doping, n-type 8.3×10^{16} cm^{-3} doping, and p-type 10^{15} cm^{-3} doping, respectively.[55]

(b) *Laser spectrum.* The center frequency ν_c of the cw Nd:YVO$_4$ laser is located at $h\nu_c = 1.165$ eV. Considering the broadening effects and the background noises, we assume the distribution of the photon energy E_l to have a pseudo-Voigt profile made of weighted contributions from Gaussian and Lorentzian distributions,[56]

$$P(E_l) = \eta_G\, G(E_l; h\nu_c, \delta_G) + (1 - \eta_G)L(E_l; h\nu_c, \delta_L),$$

where

$$G(E_l; h\nu_c, \delta_G) = \frac{1}{\delta_G\sqrt{2\pi}} \exp\left[-\frac{(E_l - h\nu_c)^2}{2\delta_G^2}\right],$$

$$L(E_l; h\nu_c, \delta_L) = \frac{1}{\pi}\left[\frac{\delta_L}{(E_l - h\nu_c)^2 + \delta_L^2}\right].$$

In the simulations we use $\eta_G = 0.8$, $\delta_G = 1$ meV, and $\delta_L = 6$ meV.

For a fixed E_l, electrons excited from different VB have different initial energy. The corresponding density of states determines the excited fraction. The total amount for each kind of excitation is proportional to $(m_c/m_v + 1)^{-3/2}\sqrt{E_l - E_{g,cv}}$ when $E_l > E_{g,cv}$, or zero otherwise. Here m_c and m_v are the effective masses of electrons and holes, respectively. The former corresponds to the Γ valley, and the latter includes $m_{hh} = 0.28m_0$ for heavy holes, $m_{lh} = 0.044m_0$ for light holes, and $m_{so} = 0.084m_0$ for split-off holes. $E_{g,cv}$ is the energy gap between edges of the two bands in the photoexcitation process.

(c) *Momentum alignment and spin-momentum correlation.* In momentum space at the instant of photoexcitation, the alignment determines the number of electrons in each direction, while the correlation assigns the corresponding average spin. Only at the Γ point do they possess simple analytical forms as shown in Table II,[1] where $\hat{\mathbf{e}}$ is the unit polarization vector ($\hat{\mathbf{p}} = i\hat{\mathbf{e}} \times \hat{\mathbf{e}}$). To generate realistic values

TABLE II. Momentum alignment and spin-momentum correlation for circular polarization at the Γ point. $\hat{\mathbf{k}}$ is the unit vector in the direction of electron momentum and $\hat{\mathbf{p}} \equiv i\,\hat{\mathbf{e}} \times \hat{\mathbf{e}}^*$ is the photon angular momentum. For relatively small wave vector, these simple forms are good approximations.[46]

Band	Heavy-hole	Light-hole	Split-off
Momentum alignment	$\frac{3}{4}[(\hat{\mathbf{p}} \cdot \hat{\mathbf{k}})^2 + 1]$	$\frac{5}{4} - \frac{3}{4}(\hat{\mathbf{p}} \cdot \hat{\mathbf{k}})^2$	1
Spin-momentum correlation	$-\dfrac{(\hat{\mathbf{p}} \cdot \hat{\mathbf{k}})\hat{\mathbf{k}}}{1 + (\hat{\mathbf{p}} \cdot \hat{\mathbf{k}})^2}$	$\dfrac{3(\hat{\mathbf{p}} \cdot \hat{\mathbf{k}})\hat{\mathbf{k}} - 2\hat{\mathbf{p}}}{5 - 3(\hat{\mathbf{p}} \cdot \hat{\mathbf{k}})^2}$	$\dfrac{1}{2}\hat{\mathbf{p}}$

when electrons are far from the valley bottom, we utilize the Kane Hamiltonian with spin-orbit coupling to calculate accurate eigenvectors. They are formulated from the Luttinger parameters $\gamma_1 = 13.35$, $\gamma_2 = 4.25$, $\gamma_3 = 5.69$ and the Kane matrix element $E_P = 26.3$ eV.[57] To construct the density matrix we first denote the eigenvectors of CB and VB, respectively, by $|c_i\rangle$ and $|v_i\rangle$, where $i \in \{1,2\}$ in each band, and $v \in \{h,l,s\}$ is comprised of heavy-hole, light-hole, and split-off bands. Then the coherent photoexcited states are $|\alpha_i(v)\rangle \propto \sum_j \{\langle c_j|\vec{\nabla}|v_i\rangle \cdot \hat{\mathbf{e}}\}|c_j\rangle$, and the density matrix is simply $\mathcal{G} = \sum_i |\alpha_i(v)\rangle\langle\alpha_i(v)|$ for electrons excited from the corresponding band. We can transform it to a 2×2 form with basis $|s\rangle$ and $|s'\rangle$, namely $\mathcal{F} = \sum_{s,s'} |s\rangle\langle s|\mathcal{G}|s'\rangle\langle s'|$, where s and s' are spin indices. Instead of what appears in Table II, the momentum alignment and spin-momentum correlation, respectively, take the forms of $\mathrm{Tr}(\mathcal{F})$ and $\mathrm{Tr}(\hat{\boldsymbol{\sigma}}\mathcal{F})$, where $\hat{\boldsymbol{\sigma}}$ denotes the Pauli matrix vector. Such numerical results still bear notable similarities to the analytical forms at the Γ point, while they indeed capture some new features such as warping effects (see Supplemental Material of Ref. 46 for figures). We use the above analysis to pregenerate tables for initial states in the simulation.

(d) *Luminescence.* It is considered when the relaxed electrons approach the valley bottom. The proper range can be estimated from the width of the direct-gap radiation peak in the PL spectra. We choose 12 meV, close to the full width at half maximum. As the electron kinetic energy drops below, radiation times are randomized according to a homogeneous Poisson process $\propto \exp(-t/\tau_{r,\Gamma})$. At the time of recombination, the density matrix of an electron with spin $\mathbf{S}$ can be reconstructed as $\mathcal{F} = [\mathcal{I} + \hat{\boldsymbol{\sigma}} \cdot \mathbf{S}]/2$.

With the aforementioned coherent state $|\alpha_i(v)\rangle \propto \sum_j \{\langle c_j|\vec{\nabla}|v_i\rangle \cdot \hat{\mathbf{e}}'\}|c_j\rangle$, we can calculate the total intensity with polarization $\hat{\mathbf{e}}'$ as follows[1]:

$$I_{\hat{\mathbf{e}}'} = \int d^3\mathbf{k} \sum_i \langle\alpha_i(v)|\mathcal{F}|\alpha_i(v)\rangle.$$

Here $|c_i\rangle$ and $|v_i\rangle$ approximate to the simple wave functions at Γ point. The circular polarization degree is defined as $\rho = (I_+ - I_-)/(I_+ + I_-)$, where I_+ and I_- are the intensities of right and left circularly polarized radiation. Especially for thermalized electrons with no spin-momentum correlation, we find that $\rho = -\mathbf{S} \cdot \hat{\mathbf{n}}'$ holds for the recombination with both heavy and light holes. Here $\mathbf{S}$ is the average spin and $\hat{\mathbf{n}}'$ is the unit vector in the observation direction of the luminescence.

B. Intrinsic scattering mechanisms

(a) *Intervalley phonon scattering.* After integrating over all possible states in the final valley, the total scattering rate reads

$$\Gamma_{iv} = \frac{D_{iv}^2 m_{d(f)}^{3/2} Z_f}{\sqrt{2}\pi\hbar^2\varrho\,\Omega_{iv}}\,\Phi_{iv}\begin{pmatrix} n_{\mathbf{q}}\sqrt{\gamma(\epsilon + \Omega_{iv} - \Delta\epsilon_{fi})} \\ (n_{\mathbf{q}}+1)\sqrt{\gamma(\epsilon - \Omega_{iv} - \Delta\epsilon_{fi})} \end{pmatrix},$$

(5)

Here and in Eq. (7) the top (bottom) line refers to phonon absorption (emission). $m_d = \sqrt[3]{m_l m_t^2}$ is the density-of-states effective mass, and (f) denotes the final valley. $\varrho = 5.32$ g/cm^3 and $n_{\mathbf{q}}$ are the crystal density and Bose-Einstein distribution, respectively. $\Phi_{iv} = 1 + 2\alpha(\epsilon \pm \Omega_{iv} - \Delta\epsilon_{fi})$ is the extra factor due to the nonparabolicity, where $\pm$ holds for top or bottom line and the same in Φ_{ac} for Eq. (7). $\Delta\epsilon_{fi}$ is the energy difference of the final and initial valley bottoms. We characterize Ge with $\Delta\epsilon_{X,L} = 0.18$ eV, $\Delta\epsilon_{X,\Gamma} = 0.04$ eV, and $\Delta\epsilon_{\Gamma,L} = 0.14$ eV. The coupling constant D_{iv} and the phonon energy Ω_{iv} of the corresponding mechanism are listed in Table III. Z_f is the number of possible final valleys. The equivalent final valley is chosen randomly. The states after scattering are equally probable on the constant energy surface with energy conservation.

(b) *Intravalley optical phonon scattering.* This effect is relatively weak in crystals with inversion symmetry. Yet we formalize it in the same way we did for the intervalley phonon scattering [when D_{op} and Ω_{op} replace, respectively, D_{iv} and Ω_{iv} in Eq. (5)]. Meanwhile, $Z_f = 1$ and $\Delta\epsilon_{fi} = 0$. For electrons in L valley, we consider $D_{op} = 5.5$ eV/Å, $\Omega_{op} = 37.1$ meV.

(c) *Intravalley acoustic phonon scattering.* We take the long wavelength approximation without distinguishing between longitudinal and transverse phonons. With the dimensionless variable

$$x = \frac{\hbar q v_s}{k_B T} \approx \frac{\hbar q^* v_s}{k_B T}\sqrt{\frac{m_d}{m_0}},$$

(6)

where $\mathbf{q} = \mathbf{k} - \mathbf{k}'$, the total scattering rate follows:

$$\Gamma_{ac} = \frac{\Xi^2 m_d^{1/2}(k_B T)^3}{2\sqrt{2}\pi\hbar^4\varrho\,v_s^4}\frac{1}{\sqrt{\gamma(\epsilon)}}\int_{x_1}^{x_2}\Phi_{ac}\begin{pmatrix} n_{\mathbf{q}} \\ n_{\mathbf{q}}+1 \end{pmatrix}x^2 dx,\quad (7)$$

TABLE III. Coupling constants and phonon energies for intervalley scattering in Ge. These values are inherited from previous works,[50,58] and can also be extracted from the empirical pseudopotential model.[59]

Scattering	XL (LA)	ΓX (LA)	ΓL (LA)	XX_g (LA)	XX_g (LO)	LL (LA, LO)	LL (TA)
D_{iv} (eV/Å)	10.0	4.06	2.0	0.789	9.46	3.0	0.20
Ω_{iv} (meV)	27.6	27.6	27.6	8.62	37.1	27.6	10.3

TABLE IV. Integration limits in Eq. (7). They guarantee the energy and momentum conservation. (See Supplemental Material of Ref. 51.)

Condition	Absorption	Emission
$\epsilon \leqslant \epsilon_s$ ($x_\epsilon \leqslant x_0$)	$x_1 = x_0 - \sqrt{x_0 x_\epsilon}$	absent
	$x_2 = x_0 + \sqrt{x_0 x_\epsilon}$	
$\epsilon > \epsilon_s$ ($x_\epsilon > x_0$)	$x_1 = 0$	$x_1 = 0$
	$x_2 = \sqrt{x_0 x_\epsilon} + x_0$	$x_2 = \sqrt{x_0 x_\epsilon} - x_0$

where $v_s = 5.4 \times 10^5$ cm/s denotes the sound velocity. The deformation potential Ξ in the L, X, and Γ valleys have values of 11, 9, and 5 eV, respectively. The integration limits x_1 and x_2 in Eq. (7) are given in Table IV where $\epsilon_s = m_d v_s^2/2$, $x_\epsilon = 4\epsilon/k_B T$, $x_0 = 4\epsilon_s/k_B T$.[51] $\Phi_{ac} = 1 + 2\alpha\epsilon \pm 2\alpha k_B T x$ is the nonparabolic factor. With the truncated Laurent expansion of phonon distribution

$$n_{\mathbf{q}}(x) = \begin{cases} 1/x - \frac{1}{2} + \frac{1}{12}x - \frac{1}{720}x^3 + \frac{1}{30240}x^5, & \text{if } x < 4, \\ 0, & \text{if } x \geqslant 4, \end{cases}$$

the integration in Eq. (7) can then be readily performed. For the state after scattering, we choose x according to the expression inside the integration in Eq. (7) with the rejection technique.[58] Then q^* is calculated from Eq. (6), and the angle between $\mathbf{k}'^*$ and $\mathbf{k}^*$ is obtained by energy and momentum conservation. The angle of rotation around $\mathbf{k}^*$ is completely random.

(d) *Rees self-scattering.* To determine the occurrence of scattering events without the difficulty of solving integral equations for each event, we use the imaginary self-scattering technique.[60,61] A homogeneous Poisson process of scattering is simulated with the rate parameter Γ_0, in which a fictitious self-scattering is included such that the total scattering rate together with the self-scattering is Γ_0. If an electron undergoes a "self-scattering" event, its wave vector immediately before and after the scattering is unchanged. This technique is valid if Γ_0 exceeds the total scattering rate of an electron in state $\mathbf{k}$. In the simulation we use $\Gamma_0 = 10^{15}$ s^{-1}.

C. Scattering mechanisms in doped samples

(a) *Ionized impurity scattering.* Using the Brooks-Herring approach,[58] we get a total scattering rate for ionized impurity with density N_I:

$$\Gamma_I = \frac{\sqrt{2} e^4 N_I m_d^{3/2}}{\pi \hbar^4 \varepsilon_0^2 \varepsilon_r^2 \beta^4} \sqrt{\gamma(\epsilon)} \, \Phi_I \left(1 + \frac{8 m_d \gamma(\epsilon)}{\hbar^2 \beta^2}\right)^{-1}, \quad (8)$$

where $\varepsilon_r = 16$ is the relative dielectric constant, and $\Phi_I = 1 + 2\alpha\epsilon$ is the nonparabolic factor. The screening β^{-1} is taken as the Debye length

$$\beta^{-1} = L_D = \sqrt{\frac{\varepsilon_0 \varepsilon_r k_B T}{N_d e^2}}. \quad (9)$$

By randomizing a number $r \in [0,1]$, the scattering angle θ follows:

$$\cos\theta = 1 - 2(1-r)\left(1 + \frac{8 m_d \gamma(\epsilon) r}{\hbar^2 \beta^2}\right)^{-1}.$$

(b) *Carrier-carrier scattering.* The interaction is between photoexcited electrons and a Fermi-Dirac distribution of thermal carriers $f(\epsilon)$ due to the background doping. We consider a screened Coulomb potential where the total scattering rate is derived from[62,63]

$$\Gamma_{cc} = \frac{e^4 N_d m_0^{3/2}}{2\pi \hbar^3 \varepsilon_0^2 \varepsilon_r^2 \mu_d^{1/2} \beta^{*2}} \int d^3 \mathbf{k}_s^* \frac{|\mathbf{g}^*|}{\beta^{*2} + \mathbf{g}^{*2}} f[\epsilon(\mathbf{k}_s^*)]. \quad (10)$$

Here $\beta^* = \beta\sqrt{\mu_d/m_0}$ and $\mu_d = (\mu_x \mu_y \mu_z)^{1/3}$, where $2\mu_i^{-1} = m_i^{-1} + m_{i(s)}^{-1}$ and $i \in \{x,y,z\}$. Parameters of thermal carriers are denoted by (s), which in the case of p-type and n-type Ge correspond to heavy holes and L-valley electrons, respectively. $g_i^* = \sqrt{m_0 \mu_i}[k_i/m_i - k_{s,i}/m_{i(s)}]$ is the transformed relative wave vector, and $\mathbf{k}_s$ is the wave vector of a thermal carrier. The integration can be evaluated numerically, and we pregenerate a table for the simulation. After a specific scattering event, $\mathbf{k}'^*$ is determined by

$$k_i'^* = \frac{1}{2} m_i \left(\frac{k_i^*}{m_i} + \frac{k_{s,i}^*}{m_{i(s)}} - \frac{g_i'^*}{\mu_i}\right),$$

where $\mathbf{k}_s$ is generated randomly from the Fermi-Dirac distribution. We notice $|\mathbf{g}'^*| = |\mathbf{g}^*|$, and the angle between $\mathbf{g}'^*$ and $\mathbf{g}^*$ is given by

$$\cos\vartheta = 1 - 2(1-r)\left(1 + r\frac{\mathbf{g}^{*2}}{\beta^{*2}}\right)^{-1},$$

with a random number $r \in [0,1]$. The azimuthal angle has no preferences from 0 to 2π.

The screening takes the form of Eq. (9) only when the energies of involved carriers are close to each other. Thus we only use Eq. (10) when the energy of the photoexcited electron is slightly (6 meV) above the defined valley bottom [within 12 meV, see Sec. III A(d)] plus the mean energy of the doped carriers. This limitation is removed if the plasmon scattering is not effective (see below). In addition, from the analysis of Eq. (10) we note that when the photoexcited electron is in the Γ valley, its much smaller effective mass compared with that of the background carrier renders the binary collision process ineffective in relaxing the photoexcited electron to the bottom of the valley (intervalley phonon-induced relaxation mechanisms become faster). The binary process is more effective in the L and X valleys where the effective masses are comparable with those of the background carriers.

(c) *Plasmon scattering.* With the plasmon-pole approximation,[64,65] we can calculate the total scattering rate

$$\Gamma_{\text{pl}} = \frac{e^3 N_d^{1/2} m_d^{1/2}}{4\sqrt{2}\pi \hbar (\varepsilon_0 \varepsilon_r)^{3/2} m_{d(s)}^{1/2}} \frac{1}{\sqrt{\gamma(\epsilon)}} \Phi_{\text{pl}} \int_{q_1^*}^{q_2^*} \frac{1}{q^*} dq^*, \quad (11)$$

where the antiderivative of the integrand is simply a logarithmic function. The nonparabolic factor is $\Phi_{\text{pl}} = 1 + 2\alpha\epsilon$. The integral interval $[q_1^*, q_2^*]$ satisfies

$$\left| \frac{1}{2q^* \sqrt{2 m_d \gamma(\epsilon)}} \left(2 m_d \omega_{\text{pl}} \sqrt{1 + \frac{q^{*2}}{\beta^2}} - \hbar q^{*2}\right) \right| \leqslant 1, \quad (12)$$

where $\omega_{\text{pl}} = (N_d e^2/m_{d(s)} \varepsilon_0 \varepsilon_r)^{1/2}$ is the plasma frequency. For the state after scattering, we choose q according to the

distribution inside the integration in Eq. (11). The angle between $\mathbf{q}^*$ and $\mathbf{k}^*$ is determined by energy conservation, in which the electron loses the energy of $\hbar\omega_{pl}\sqrt{1+(q^*/\beta)^2}$, and the azimuthal angle is completely random. Eventually we obtain $\mathbf{k}'^* = \mathbf{k}^* + \mathbf{q}^*$.

We notice that Eq. (12) is not always possible, especially when $\epsilon \lesssim \hbar\omega_{pl}$. In this case we broaden the suitable range of the binary carrier-carrier scattering to avoid discontinuity. We note that the restriction $\epsilon \lesssim \hbar\omega_{pl}$ can be readily achieved in the Γ valley due to its small effective mass (compared with the L and X valleys).

IV. PHYSICAL PICTURE

Here we highlight the underlying physics leading to the results outlined in the previous experimental and theoretical sections. Following the photoexcitation of spin-polarized electrons in the Γ valley, their vast majority relax to the bottom of the L valleys, located $\Delta\epsilon_{\Gamma,L} \simeq 0.14$ eV below the edge of the Γ valley. The lifetime of electrons in the L valley is relatively long (>1 μs) and governed by nonradiative recombination channels across the indirect band gap. Our work, however, focuses on the minute fraction of electrons that experience direct-gap radiative recombination from the bottom of the Γ valley. The circular polarization degree of this luminescence provides useful information on the dominant relaxation mechanisms of photoexcited electrons.

The results from experiments and theory summarized in Figs. 3(b) and 4 show a strong decay of the circular polarization degree at high temperatures. We can infer that radiative recombination of unpolarized electrons already plays a role at 120 K and it dominates the luminescence above 170 K. The source of these unpolarized electrons is from thermal activation of L valley electrons. Specifically, electrons from the bottom of the L valleys can visit the Γ valley with a probability of $\sim\exp(-\Delta\epsilon_{\Gamma,L}/k_B T)$. During these sporadic visits there is a minute probability for the electrons to experience radiative recombination rather than phonon-induced ultrafast scattering back to the L valley. Given that the recombination lifetime of electrons in the L valley is longer than 1 μs and that their spin relaxation time is of the order of 1 ns at high temperatures,[18] the majority of the ultrashort visits in the Γ valley take place when the electrons are no longer spin polarized.

Below $\sim$120 K, the aforementioned thermal-activation process is practically quenched, and the luminescence has contributions from two types of spin-polarized electron populations. The first is of electrons excited from the SO, which results from the finite energy width of the laser excitation (see Sec. III A). These electrons are excited at the bottom of the Γ valley and in what follows we term them "low-energy" electrons. As expected from the selection rules,[2] upon radiative recombination they provide a circular polarization degree of $+50\%$. The second population is of electrons excited from heavy and light hole VB. These electrons need to relax more than 100 meV before reaching the bottom of the Γ valley and in what follows we term them "high-energy" electrons. Only after this energy relaxation, their average contribution of -25% to the circular polarization degree[2] can be noticed in the peak of the direct band gap PL.

The relative contributions of low-energy and high-energy electron populations to the direct-gap luminescence strongly depend on excitation, temperature, and doping conditions. Figures 3(b) and 4 show that below 50 K the circular polarization degrees are relatively constant and their doping-dependent values range from $\sim-10\%$ in p^+-Ge to nearly $\sim+30\%$ in i-Ge. In between 50 and 120 K, the circular polarization degree of all samples increases reaching nearly $+50\%$ in the intrinsic sample. The change in behavior around $\approx$50 K is attributed to the excitation conditions, as discussed in Sec. II B. The density of low-energy electrons can significantly increase at higher temperatures because of the band gap shrinkage and because carrier-carrier interactions become relevant. This increase explains the behavior of the circular polarization degree above 50 K in all samples, where a value of $+50\%$ indicates that only these electrons contribute to the direct band gap luminescence. At temperatures below 50 K, the density of low-energy electrons is low and relatively constant given the fact that the energy band gap shrinks only by $\sim$3 meV from zero to 50 K. See Sec. III A for the analysis of the laser line and excitation conditions.

The density of high-energy electrons reaching the bottom of the Γ valley after relaxation strongly depends on doping conditions. In the intrinsic sample, the energy relaxation of high-energy electrons is governed by phonon-induced intervalley scattering between Γ, X, and L valleys, where after each phonon emission the electron lose a few tens of meV. Since it is highly likely for high-energy electrons to be transferred out of the Γ valley during such energy relaxation, the direct-gap luminescence is governed by low-energy electrons. This physics explains the positive and high circular polarization degree from the intrinsic sample at low temperatures (in spite of the relatively small population of low-energy electrons at these temperatures). In the doped samples, on the other hand, the energy relaxation of high-energy electrons is governed by collisions with the background carriers. These Coulomb collisions come from a binary process in which a photoexcited electron collides with a background carrier,[62,63] and also a collective process in which the photoexcited electron interacts with the thermal plasma of background carriers.[64,65]

The energy relaxation of photoexcited electrons due to Coulomb collisions is effective in the X and L valleys but not in the Γ valley. This difference stems from the effective mass as explained in Sec. III C. A typical scenario at low temperatures is that photoexcited electrons in the Γ valley experience phonon-induced intervalley scattering to one of the X valleys since it has higher rate compared with scattering to the L valleys.[30] The hot electrons then thermalize to the bottom of the X valley via the plasmon and carrier-carrier scattering mechanisms. The phonon-induced intervalley scattering typically takes place after electrons reach the bottom of the X valley transferring some of the electrons back to the Γ valley, whereas most scatter to the L valley. Since $\Delta\epsilon_{X,\Gamma} \simeq 40$ meV, electrons that scatter back to the Γ valley reach the valley bottom where they can effectively contribute to the direct band gap luminescence. These characteristics lead to the similarity between the curves of the fairly doped samples, despite the big gap in the doping level of n-Ge and p^+-Ge, namely 8.3×10^{16} and 3.6×10^{18} cm^{-3}. For p^--Ge (10^{15} cm^{-3}), the plasmon scattering is negligible, and the binary

carrier-carrier scattering is not as efficient at low temperatures. Its circular polarization degree is therefore located in between the heavily doped and intrinsic samples, as expected.

Finally, we note that the cooling process in the X valley mediated by background impurities is expected to lead to an increase of the direct-gap emission with the doping level. Such a general result has to take place in both n- and p-doped Ge samples. In the former, this contribution sums up to the higher electron population due to the increased Fermi level with n-type doping.[66]

V. CONCLUSIONS

In this work we have reported a joint experimental and theoretical study of the polarization of light emitted in transitions across the direct band gap of bulk Ge. The optical investigation, based upon polarimetric analysis, provides compelling confirmation that optical orientation of carrier spin can be achieved in bulk Ge. The detailed analysis of the state of light polarization further demonstrates that the degree and helicity of direct-gap emission remarkably depend upon parameters such as doping and temperature.

We emphasize that by combining continuous-wave polarization-resolved PL experiments and Monte Carlo calculations, we gather simultaneous information about spin and carrier relaxation mechanisms, without relying on time resolved techniques. Indeed, in the optical orientation process, electrons are photogenerated in the Γ valley from optically coupled heavy hole or split-off valence band states at different energies and with opposite spin orientation. Such information does not get wiped out during the subsequent radiative recombination, because, owing to the ultrafast lifetime of Γ electrons,[30] it remains encoded in the angular momentum of the emitted light. As a result, the measurement of the helicity and polarization degree of the band-edge luminescence allows us to keep track of the dominant nonequilibrium spin-polarized population of electrons experiencing radiative recombination, and to infer important information about energy and spin relaxation channels. Thermal activation of unpolarized L valley electrons is shown to explain the luminescence depolarization at high temperatures, whereas the doping level accounts for the different state of light polarization in the low temperature regime. Finally, our findings point out the pivotal impact in the cooling process of hot electrons played by carrier-plasmon scattering within the X valleys, whose role in defining carrier

dynamics has been largely overlooked in many of the previous literature works dealing with direct-gap luminescence in Ge.

The study of the injection of spin-polarized carriers and of circularly polarized emission at the direct gap of Ge is important also application wise. We anticipate that a systematic calibration in the low temperature regime of the dependence of the polarization degree ρ upon doping can possibly lead to the development of a diagnostic tool for the determination of the impurity content in Ge. Such spectroscopic method is nondestructive and has a high spatial resolution ($\approx \mu$m). In addition, it does not require accurate sample preparation and can be applied to address a doping range not easily accessible by conventional techniques, e.g., energy dispersive x-ray spectroscopy.

Finally, the recently discovered lasing action in Ge on Si heterostructures,[9,67] albeit debated,[68–71] holds the promise of laser sources monolithically integrated onto the mainstream CMOS platform,[10] thus filling the gap for the development of the active devices needed to ground Si photonics. At present, however, direct-gap electroluminescence[72–75] and lasing[67] in Ge-based heterostructures have been achieved only under high current densities and shown to be not efficient yet.[70,75] Such drawbacks strongly hamper the widespread application of Ge-based light sources.

We suggest, however, that pursuing the concept of spin-based Ge emitters can provide a sizable improvement in this field.[76–79] Pumping spin-polarized carriers in the optical gain medium by using spin selective contacts or circularly polarized light can reduce the injection threshold required for electroluminescence or lasing action, finally boosting the performances of the Ge emitters and their implementation into Si-photonics circuits.

ACKNOWLEDGMENTS

---

*The first two authors have equal contribution to this work; Correspondence should be addressed to: fabio.pezzoli@unimib.it

[1] M. I. Dyakonov and V. I. Perel, in *Optical Orientation*, edited by F. Meier and B. P. Zakharchenya (North-Holland, New York, 1984), Chap. 2.

[2] I. Zutic, J. Fabian, and S. Das Sarma, Rev. Mod. Phys. **76**, 323 (2004).

[3] I. Zutic, J. Fabian, and S. C. Erwin, Phys. Rev. Lett. **97**, 026602 (2006).

[4] P. Li and H. Dery, Phys. Rev. Lett. **105**, 037204 (2010).

[5] P. S. Fodor and J. Levy, J. Phys.-Condens. Mat. **18**, S745 (2006).

[6] I. Appelbaum, B. Huang, and D. J. Monsma, Nature (London) **447**, 295 (2007).

[7] S. A. Wolf, D. D. Awschalom, R. A. Buhrman, J. M. Daughton, S. von Molnar, M. L. Roukes, A. Y. Chtchelkanova, and D. M. Treger, Science **294**, 1488 (2001).

[8] M. W. Wu, J. H. Jiang, and M. Q. Weng, Phys. Rep. **493**, 61 (2010).

[9] J. Liu, X. Sun, R. Camacho-Aguilera, L. C. Kimerling, and J. Michel, Opt. Lett. **35**, 679 (2010).

[10] D. Liang and J. E. Bowers, Nat. Photon. **4**, 511 (2010).

[11] E. J. Loren, B. A. Ruzicka, L. K. Werake, H. Zhao, H. M. van Driel, and A. L. Smirl, Appl. Phys. Lett. **95**, 092107 (2009).

[12]M. Virgilio and G. Grosso, Phys. Rev. B **80**, 205309 (2009).

[13]C. Guite and V. Venkataraman, Phys. Rev. Lett. **107**, 166603 (2011).

[14]F. Pezzoli, F. Bottegoni, D. Trivedi, F. Ciccacci, A. Giorgioni, P. Li, S. Cecchi, E. Grilli, Y. Song, M. Guzzi *et al.*, Phys. Rev. Lett. **108**, 156603 (2012).

[15]S. Zwerdling, B. Lax, L. M. Roth, and K. J. Button, Phys. Rev. **114**, 80 (1959).

[16]J. Rioux and J. E. Sipe, Phys. Rev. B **81**, 155215 (2010).

[17]E. J. Loren, J. Rioux, C. Lange, J. E. Sipe, H. M. van Driel, and A. L. Smirl, Phys. Rev. B **84**, 214307 (2011).

[18]P. Li, Y. Song, and H. Dery, Phys. Rev. B **86**, 085202 (2012).

[19]P. Li, D. Trivedi, and H. Dery, Phys. Rev. B **87**, 115203 (2013).

[20]T. Uemura, K. Kondo, J. Fujisawa, K.-i. Matsuda, and M. Yamamoto, Appl. Phys. Lett. **101**, 132411 (2012).

[21]A. Jain, J. C. Rojas-Sanchez, M. Cubukcu, J. Peiro, J. C. Le Breton, E. Prestat, C. Vergnaud, L. Louahadj, C. Portemont, C. Ducruet *et al.*, Phys. Rev. Lett. **109**, 106603 (2012).

[22]C. Guite and V. Venkataraman, Appl. Phys. Lett. **101**, 252404 (2012).

[23]C. Hautmann and M. Betz, Phys. Rev. B **85**, 121203(R) (2012).

[24]Y. Song and H. Dery, Phys. Rev. B **86**, 085201 (2012).

[25]O. D. Restrepo and W. Windl, Phys. Rev. Lett. **109**, 166604 (2012).

[26]D. H. Goldstein, *Polarized Light* (Taylor-Francis, London, 2010).

[27]E. Collett, *Field Guide to Polarization* (SPIE, Bellingham, WA, 2005).

[28]Y. P. Varshni, Physica **34**, 149 (1967).

[29]T. Nishino and Y. Hamakawa, J. Phys. Soc. Jpn. **26**, 403 (1969).

[30]X. Q. Zhou, H. M. van Driel, and G. Mak, Phys. Rev. B **50**, 5226 (1994).

[31]G. Mak and H. M. van Driel, Phys. Rev. B **49**, 16817 (1994).

[32]D. W. Bailey and C. J. Stanton, J. Appl. Phys. **77**, 2107 (1995).

[33]K. Kolata, N. S. Köster, A. Chernikov, M. J. Drexler, E. Gatti, S. Cecchi, D. Chrastina, G. Isella, M. Guzzi, and S. Chatterjee, Phys. Rev. B **86**, 201303 (2012).

[34]P. Y. Yu and M. Cardona, *Fundamentals of Semiconductors: Physics and Materials Properties* (Springer, Heidelberg, 2010), Chap. 3.

[35]J. Pankove, *Optical Processes in Semiconductors* (Dover, New York, 1971), Chap. 6.

[36]R. R. Lieten, K. Bustillo, T. Smets, E. Simoen, J. W. Ager, III, E. E. Haller, and J.-P. Locquet, Phys. Rev. B **86**, 035204 (2012).

[37]J. Wagner and L. Viña, Phys. Rev. B **30**, 7030 (1984).

[38]K. Tanaka, H. Ohtake, and T. Suemoto, Phys. Rev. B **50**, 10694 (1994).

[39]C. Haas, Phys. Rev. **125**, 1965 (1962).

[40]P. Grande, A. Hentz, R. Pezzi, I. Baumvol, and G. Schiwietz, Nucl. Instrum. Methods Phys. Res. B **256**, 92 (2007).

[41]C. Hautmann, B. Surrer, and M. Betz, Phys. Rev. B **83**, 161203(R) (2011).

[42]R. R. Parsons, Phys. Rev. Lett. **23**, 1152 (1969).

[43]In p^+-Ge a high energy features at 1.047 eV can be observed at 4 K. Its energy and angular momentum is consistent with the one discussed in Ref. 37.

[44]K. Tanaka, H. Ohtake, and T. Suemoto, Phys. Rev. Lett. **71**, 1935 (1993).

[45]G. K. Wertheim, M. A. Butler, K. W. West, and D. N. Buchanan, Rev. Sci. Instrum. **45**, 1369 (1974).

[46]L. Qing, Y. Song, and H. Dery, Phys. Rev. Lett. **107**, 107202 (2011).

[47]V. D. Dymnikov, M. I. Dyakonov, and N. I. Perel, Sov. Phys. JETP **44**, 1252 (1976).

[48]A. V. Efanov and M. V. Entin, Phys. Status Solidi B **118**, 63 (1983).

[49]E. O. Kane, J. Phys. Chem. Solids **1**, 249 (1957).

[50]C. Jacoboni, F. Nava, C. Canali, and G. Ottaviani, Phys. Rev. B **24**, 1014 (1981).

[51]J. Li, L. Qing, H. Dery, and I. Appelbaum, Phys. Rev. Lett. **108**, 157201 (2012).

[52]M. Lundstrom, in *Modular Series on Solid State Devices*, edited by G. W. Neudeck and R. F. Pierret (Addison-Wesley, New York, 1990), Vol. 10.

[53]E. M. Conwell and M. O. Vassell, Phys. Rev. **166**, 797 (1968).

[54]C. Herring and E. Vogt, Phys. Rev. **101**, 944 (1956).

[55]S. C. Jain and D. J. Roulston, Solid-State Electron. **34**, 453 (1991).

[56]P. Thompson, D. E. Cox, and J. B. Hastings, J. Appl. Crystallogr. **20**, 79 (1987).

[57]L. C. Lew Yan Voon and M. Willatzen, *The k·p Method: Electronic Properties of Semiconductors* (Springer, Berlin, 2009), Appendix C.

[58]C. Jacoboni and L. Reggiani, Rev. Mod. Phys. **55**, 645 (1983).

[59]J. R. Chelikowsky and M. L. Cohen, Phys. Rev. B **14**, 556 (1976).

[60]H. D. Rees, Phys. Lett. A **26**, 416 (1968).

[61]H. D. Rees, J. Phys. Chem. Solids **30**, 643 (1969).

[62]J. Dewey and M. A. Osman, Appl. Phys. Lett. **62**, 187 (1993).

[63]H. Dery, B. Tromborg, and G. Eisenstein, Phys. Rev. B **67**, 245308 (2003).

[64]H. Haug and S. W. Koch, *Quantum Theory of the Optical and Electronic Properties of Semiconductors*, 3rd ed. (World Scientific, Singapore, 1990), Chap. 8.

[65]G. D. Mahan, *Many Particle Physics*, 3rd ed. (Plenum, New York, 2000), Chap. 5.

[66]X. Sun, J. Liu, L. C. Kimerling, and J. Michel, Appl. Phys. Lett. **95**, 011911 (2009).

[67]R. E. Camacho-Aguilera, Y. Cai, N. Patel, J. T. Bessette, M. Romagnoli, L. C. Kimerling, and J. Michel, Opt. Express **20**, 11316 (2012).

[68]L. Carroll, P. Friedli, S. Neuenschwander, H. Sigg, S. Cecchi, F. Isa, D. Chrastina, G. Isella, Y. Fedoryshyn, and J. Faist, Phys. Rev. Lett. **109**, 057402 (2012).

[69]C. Boztug, J. R. Sanchez-Perez, F. F. Sudradjat, R. B. Jacobson, D. M. Paskiewicz, M. G. Lagally, and R. Paiella, Small **9**, 622 (2013).

[70]B. Dutt, D. S. Sukhdeo, D. Nam, B. M. Vulovic, Z. Yuan, and K. C. Saraswat, IEEE Photon. J. **4**, 2002 (2012).

[71]X. Wang, L. C. Kimerling, J. Michel, and J. Liu, Appl. Phys. Lett. **102**, 131116 (2013).

[72]W. Hu, B. Cheng, C. Xue, H. Xue, S. Su, A. Bai, L. Luo, Y. Yu, and Q. Wang, Appl. Phys. Lett. **95**, 092102 (2009).

[73]P. Chaisakul, D. Marris-Morini, G. Isella, D. Chrastina, N. Izard, X. Le Roux, S. Edmond, J. R. Coudevylle, and L. Vivien, Appl. Phys. Lett. **99**, 141106 (2011).

[74]K. Gallacher, P. Velha, D. J. Paul, S. Cecchi, J. Frigerio, D. Chrastina, and G. Isella, Appl. Phys. Lett. **101**, 211101 (2012).

[75]N. Donguk, D. Sukhdeo, C. Szu-Lin, A. Roy, K. C. Y. Huang, M. Brongersma, Y. Nishi, and K. Saraswat, Appl. Phys. Lett. **100**, 131112 (2012).

[76]J. Rudolph, D. Hägelea, H. M. Gibbs, G. Khitrova, and M. Oestreich, Appl. Phys. Lett. **82**, 4516 (2003).

[77]M. Holub, J. Shin, D. Saha, and P. Bhattacharya, Phys. Rev. Lett. **98**, 146603 (2007).

[78]M. Holub and B. T. Jonker, Phys. Rev. B **83**, 125309 (2011).

[79]J. Lee, R. Oszwaldowski, C. Gøthgen, and I. Žutić, Phys. Rev. B **85**, 045314 (2012).